# Automatic Fuzzy Cognitive Maps for Explainable Image-based Pneumonia Detection

Georgia Sovatzidi
Department of Computer Science and Biomedical Informatics, University of Thessaly
gsovatzidi@uth.gr

Michael D. Vasilakakis
Department of Computer Science and Biomedical Informatics, University of Thessaly
vasilaka@uth.gr

Dimitris K. Iakovidis
Department of Computer Science and Biomedical Informatics, University of Thessaly
diakovidis@uth.gr

## ABSTRACT

Pneumonia has a significant impact on morbidity and mortality worldwide and is associated with serious diseases, such as coronavirus disease 2019 (COVID-19). Pneumonia diagnosis is typically performed by medical experts, trained to evaluate chest x-rays, which is usually a difficult and time-consuming task. To address this problem, in this paper, a novel classification scheme based on a Fuzzy Cognitive Map (FCM) is introduced. The proposed FCM model is applied for the detection of foci of consolidation, which is a common radiographic manifestation of pneumonia, while enabling the explanation of the outcome using linguistic terms. Also, unlike most FCM models, it is automatic, in the sense that it does not require any manual intervention for the construction of the fuzzy graph. Experimental results using publicly available datasets demonstrate the effectiveness of the introduced model.

## CCS CONCEPTS

• **Computing methodologies**; • **Artificial intelligence**; • **Knowledge representation and reasoning**; • **Vagueness and fuzzy logic**;

## KEYWORDS

Fuzzy logic, fuzzy cognitive maps, pneumonia, x-rays, explainability

**ACM Reference Format:**
Georgia Sovatzidi, Michael D. Vasilakakis, and Dimitris K. Iakovidis. 2023. Automatic Fuzzy Cognitive Maps for Explainable Image-based Pneumonia Detection. In *27th Pan-Hellenic Conference on Progress in Computing and Informatics (PCI 2023), November 24–26, 2023, Lamia, Greece.* ACM, New York, NY, USA, 5 pages. https://doi.org/10.1145/3635059.3635071

## 1 INTRODUCTION

Pulmonary infections can be evoked by various pathogens including fungi, bacteria, and viruses, which can be fatal and cause serious problems, particularly among immunocompromised people. Pneumonia is a heterogeneous and complex disease that occurs when a virulent pathogen, such as S. pneumoniae and SARS-CoV-2, invades the normally sterile space in the lungs [1]. For the diagnosis of pneumonia, chest x-ray is the most commonly used method. However, this method can be time consuming, as pneumonia has similar opacity to images with other diseases such as lung cancer and excess fluid. Thus, despite advances in the treatment and prevention of pneumonia, further improvement in the diagnosis of respiratory diseases, including pneumonia, remains a challenge.

Recently, artificial intelligence has been effectively utilized to detect respiratory diseases [2]. Specifically, FCMs [3] constitute a soft computing technique that is used to model complex systems and provide results that are compatible to human logic. Among various soft computing approaches, FCMs have shown remarkable results used as a tool aimed at modeling and analyzing the dynamics of complex systems. The simplicity and effectiveness of FCMs have contributed to be widely used in many applications of various scientific domains [4], including time series forecasting, development of medical decision support systems [5], and medical decision making tasks [6] [8].

In this paper, we introduce a graph-based model, which is applied for image-based pneumonia detection. The proposed FCM model receives chest x-ray images of patients as an input, and it classifies them as belonging to a normal or pneumonia case, based on the texture of the lung regions. Unlike most current FCM models, the proposed one is automatically constructed, without the need of manual input by medical experts, because the weights of the FCM are automatically adjusted. More importantly, the proposed model provides explainable results, by providing a humanly-understandable reasoning regarding the reasons of inferring its output. Thus, the proposed model does not only offer an approach towards the reduction of diagnostic errors and the productivity increase of the experts, but also a tool that can offer more reliable outcomes for the experts based on causal reasoning. The rest of the paper is organized into four sections. Section 2 includes the basic theory of FCMs, section 3 presents the proposed model, and section 4 describes the experiments and results obtained for the case study of pneumonia detection in x-ray images. Finally, the conclusions derived from this study are summarized in section 5.

## 2 FUZZY COGNITIVE MAPS

Fuzzy Cognitive Maps originate from the combination of fuzzy logic and neural networks and constitute illustrative model representations close to human perception [3]. An FCM is a weighted graph consisting of nodes and links among them. Each node represents a concept $C = C_1, C_2, ..., C_n$where n is the total number of concepts and form a state vector $A = \{A_r\}$.The causal-effect relationships among them are described by directed weighted edges. The edge weight $w_{ji}$ is a fuzzy value representing the impact that a concept


*PCI 2023, November 24–26, 2023, Lamia, Greece*

ACM ISBN 979-8-4007-1626-3/23/11…$15.00
https://doi.org/10.1145/3635059.3635071

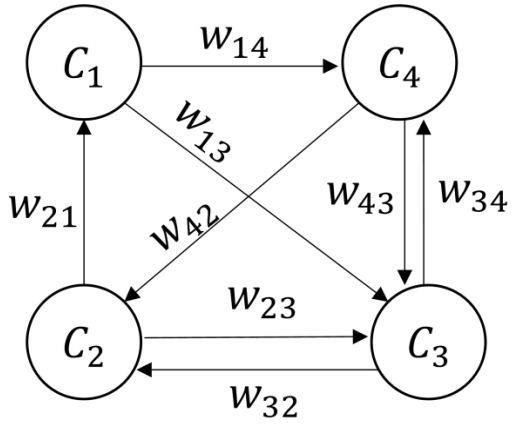


**Figure 1: Example of FCM with four concepts**

$C_j$has on the connected other concept $C_i$. For example, according to Figure 1, looking at $C_1 \rightarrow C_4$, $C_1$ has an impact on $C_4$ , described by $w_{14}$. Based on the sign of the weight, this interaction can be negative, positive, or neutral [3]. The weights ranging within $[-1, 1]$, constitute a square weight matrix $W$.

For the definition of an FCM, experts with specific scientific knowledge are involved in the determination of concepts and their interconnections, utilizing fuzzy "IF-THEN" rules. The FCM is updated iteratively, until either the system converges, or meets a stopping criterion, such as reaching a predefined number of iterations. The concept values $A_i^{t+1}$ at a next iteration $(t+1)$, are calculated taking into consideration the concept values $A_i^t$ of the previous iteration $t$, as follows:

$$A_i^{t+1} = f\left(A_i^t + \sum_{j=1, j\neq i}^{n} w_{ji} A_j^t\right) \tag{1}$$

where $t = 1 \ldots., T$ is the iteration, $w_{ji}$ is the weight matrix of the edge connecting $C_j$ to$C_i$, and $f$ is a sigmoid transfer function, such as the log sigmoid function [3]. The initial state vector represents the FCM input concept values for t=0, and is defined as $A^0 = (A_1^0, \ldots, A_n^0)$.

## 3 AUTOMATICALLY CONSTRUCTED FUZZY COGNITIVE MAPS

To examine the lungs using the introduced model, a segmentation of an x-ray image into 6 regions is performed, based on [7]. Specifically, the division of lungs was done into six main zones, utilizing two lines as borders; line A was defined at the level of inferior wall of the aortic arch, and line B was drawn at the level of the inferior wall of the right inferior pulmonary vein. Thus, six lung regions evoked; in the upper, middle and lower zones of the left and right lung [7]. Taking the above into consideration, the lung regions that evoke are the following: Left Up, Middle and Low (LU, LM, LL) and Right Up, Middle, and Low (RU, RM, RL), as presented in Figure 2 (a).

### 3.1 Figures

In order to perform pneumonia diagnosis in x-ray images, textural features firstly need to be extracted. For that purpose, the energy from different bands of the single level 2D-Discrete Wavelet Transform (2D-DWT) are calculated [8], [9]. Specifically, a separable filter-bank is applied to the original image $I_0$ according to Eq. 2).

$$\left.\begin{aligned} I_{j0} &= \left[H_x * \left(H_y * I_{j0-1}\right)_{\downarrow 2,1}\right]_{\downarrow 1,2} \\ D_{j1} &= \left[H_x * \left(G_y * I_{j0-1}\right)_{\downarrow 2,1}\right]_{\downarrow 1,2} \\ D_{j2} &= \left[G_x * \left(H_y * I_{j0-1}\right)_{\downarrow 2,1}\right]_{\downarrow 1,2} \\ D_{j3} &= \left[G_x * \left(G_y * I_{j0-1}\right)_{\downarrow 2,1}\right]_{\downarrow 1,2} \end{aligned}\right\} \tag{2}$$

where $k \in Z$,$1 \leq j \leq j_0$, , $j_0 \in Z$, $\downarrow 2,1$ and $\downarrow 1,2$ represent the subsampling along the rows and columns respectively, (*) is the convolution operator, $H$ is the low-pass filter. The variable $G$ corresponds to the high-pass filter. Thus, the energy from band $I_{j_0}$, of the DWT is calculated, for different DWT families and are utilized as a feature to represent the contents of the chest x-ray images. The extracted feature vector that describes the energy values in an image region is symbolized as $E_\lambda^r = (e_1,\ e_2, \ldots, e_u)$, where $u$ represents the different wavelet families, *e.g.,* Haar, Daubechies [10] , $\lambda = 1, 2, \ldots, \Lambda$ is an identifier corresponding to the examined classes, *e.g.* Normal lungs, lungs with Pneumonia. The variable $r = 1, 2,\ \ldots,\ R$ represents the examined lung regions. Specifically, for this study, a total number of $R = 6$ lung regions were used for the experiments, based on [7], as presented in Figure 2.

### 3.2 Fuzzy Set Construction

To linguistically describe the energy level of lung regions in each image, fuzzy sets are defined and constructed accordingly for each extracted feature $e_u$. Specifically, the average value $\bar{e}_u$ for $N_\lambda$ training images of each class $\lambda$ is calculated, based on Eq. 3):

$$\bar{e}_u = \frac{\sum_{N_\lambda} e_u}{N_\lambda} \tag{3}$$

with a standard deviation $\sigma(\bar{e}_u)$. A fuzzy set $s_{u,\lambda}^r$ is defined based on $\bar{e}_u$, $\sigma(\bar{e}_u)$ with a respective membership function:

$$0 < \mu_{u,\lambda}^r\left(e_u\right) < 1 \tag{4}$$

For simplicity, triangular membership functions are used. The fuzzy sets $(s_{u,\lambda}^r)$ of the same class region $r$ are then aggregated using the fuzzy union operation, resulting into new fuzzy sets $s_\lambda^r$, each of which corresponds to a feature $e_u$, with a membership function $\mu_\lambda^r(e_u)$. The overall energy $\widehat{E^r}$ of each image region $r$ is calculated as follows:

$$\widehat{E^r} = \frac{\sum_{i=1}^{u} e_u \cdot max\left(\mu_{u,1}^r\left(e_u\right), .., \mu_{u,\Lambda}^r\left(e_u\right)\right)}{\sum_{i=1}^{u} max\left(\mu_{u,1}^r\left(e_u\right), .., \mu_{u,\Lambda}^r\left(e_u\right)\right)} \tag{5}$$

Thus, based on Eq.(5) the initial state vector takes the following form:

$$A^0\left(\widehat{E^r}\right) = \max\left(\mu_1^r\left(\widehat{E^r}\right), .., \mu_\Lambda^r\left(\widehat{E^r}\right)\right) \tag{6}$$

which is then scaled in the range of $[arg\max(\mu_1^r(\widehat{E^r}), .., \mu_\Lambda^r(\widehat{E^r})) - 1/\Lambda, arg\max(\mu_1^r(\widehat{E^r}), .., \mu_\Lambda^r(\widehat{E^r}))/\Lambda]$.

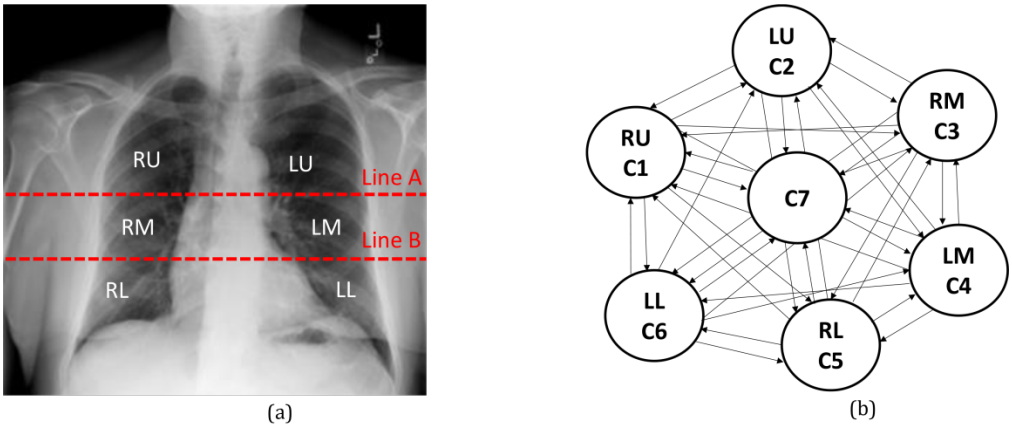


(a) (b)

**Figure 2: (a) Segmentation of lungs into six regions: Left Upper, Middle, Lower (LU, LM, LL) and Right Upper, Middle, Lower (RU, RM, RL), (b) Structure of the proposed FCM model.**

### 3.3 Definition of Interconnections

FCMs represent knowledge through concepts and directed, weighted edges between them [3]. In this study, to diagnose pneumonia, a total of seven initial concepts, representing the lung regions (Figure 2) were considered. Specifically, the structure of the proposed model for the pneumonia diagnosis problem is illustrated in Figure 2 (b); $C_1$=Right Upper (RU), $C_2$= Left Upper (LU), $C_3$= Right Middle (RM), $C_4$= Left Middle (LM), $C_5$= Right Lower (RL), $C_6$= Left Lower (LL), and $C_7$= Pneumonia, which is the output node that determines the final outcome.

To estimate the weight matrix of the graph, the causal relationships between the concepts are examined. Initially, the calculation of the weights between an input concept $C_r$ and the output concept $C_7$ of the graph is performed based on Eq. 7).

$$w_{C_r|C_7} = \frac{R^r_{\lambda 1} - R^r_{\lambda 2}}{R^r_{\lambda 1} + R^r_{\lambda 2}} \tag{7}$$

where $\lambda_1, \lambda_2$ are the classes belonging to different types of x-ray images, *i.e.*, Normal, Pneumonia, respectively. Equation 7 expresses the energy rate. The weighted average energy is calculated using Eq.(8). This average value characterizes the calculated energy level among the lung regions

$$R^r_\lambda = \frac{\sum_{k=1}^{K_\lambda} \widehat{E^r} \cdot max\left(\mu^r_{\lambda_1}\left(\widehat{E^r}\right), \mu^r_{\lambda_2}\left(\widehat{E^r}\right)\right)}{\sum_{k=1}^{K_\lambda} max\left(\mu^r_{\lambda_1}\left(\widehat{E^r}\right), \mu^r_{\lambda_2}\left(\widehat{E^r}\right)\right)} \tag{8}$$

Then, the influence between two concepts which represent the energy level in two lung regions $C_{r_1}$, $C_{r_2}$ , can be defined with respect to the differences observed in the certain regions and is calculated based on Eq. 9).

$$w_{C_{r_1}|C_{r_2}} = \frac{R^{r_1}_{\lambda_1} - R^{r_1}_{\lambda_2} + R^{r_2}_{\lambda_1} - R^{r_2}_{\lambda_2}}{R^{r_1}_{\lambda_1} + R^{r_1}_{\lambda_2} + R^{r_2}_{\lambda_1} + R^{r_2}_{\lambda_2}} \tag{9}$$

where $r_1, r_2$ are the lung regions, and $\lambda_1, \lambda_2$ correspond to the classes belonging to different types of x-ray images.

## 4 EXPERIMENTS AND RESULTS

### 4.1 Dataset Description and Processing

The dataset used for the experiments includes 5247 chest X-ray images of normal, viral and bacterial pneumonia. Specifically, 3906 images correspond to patients suffering from pneumonia (2561 images for bacterial pneumonia and 1345 for viral pneumonia) and 1341 images are normal chest x-ray images. The resolution of the images varies from 400p to 2000p [13]. In addition, a total of 10 variations of this dataset was created, by following a 10-fold cross validation of the samples into non-overlapping training and test subsets [14].

### 4.2 Classification Results

To evaluate the performance of the proposed model the following metrics were utilized: accuracy, sensitivity, specificity, and Area under the ROC Curve (AUC) [14], [15].

$$Accuracy = \frac{TP + TN}{TP + TN + FP + FN} \tag{10}$$

$$Sensitivity = \frac{TP}{TP + FN} \tag{11}$$

$$Specificity = \frac{TN}{TN + FP} \tag{12}$$

TP: True Positive, TN: True Negative, FP: False Positive, FN: False Negative

The proposed FCM was compared to the following well-known classifiers: Support Vector Machine (SVM), k-Nearest Neighbors (k-NN) algorithm, Naïve Bayes (NB), Binary Decision Tree (BDT) [11] and the results are presented in Table I. The ranges of the hyperparameters tested in the case of the SVM classifiers were $C = [10^{-2}, 10^2]$, $\gamma = [10^{-3}, 10^3]$, and for KNN the range of nearest neighbors was [1, 5]. As can be observed from Table 1, the proposed FCM model provides higher results compared to the rest models. Specifically, the introduced model achieved an accuracy of 93%, with a sensitivity of 51% and a specificity of 98%. The calculated area under the ROC curve (AUC) was equal to 93%. In addition, it has to be mentioned that an advantage over the rest compared

**Table 1: Comparisons of the proposed FCM model with well-known classifiers.**

| Models/Metrics | Accuracy | AUC | Sensitivity | Specificity |
|---|---|---|---|---|
| SVM | 0.90 | 0.90 | 0.38 | 0.97 |
| $k$-NN | 0.89 | 0.88 | 0.38 | 0.97 |
| NB | 0.66 | 0.68 | 0.80 | 0.64 |
| BDT | 0.90 | 0.89 | 0.39 | 0.96 |
| Proposed FCM | **0.93** | **0.93** | **0.51** | **0.98** |

methods is that the proposed model provides outcomes that are understandable in a way compatible to human logic.

### 4.3 Explainable Example of Pneumonia Detection

For better understanding the interpretation of the outcome derived from the proposed FCM model, an indicative example of pneumonia detection is presented. Firstly, an x-ray image of the dataset used was randomly selected and inserted as input of the proposed model. Using Eq. 6) the initial state vector of the graph, for the given problem, was calculated and defined as follows: $A^0$ = (0.90, 0.80, 0.87, 0.87, 0.41, 0.39, 0). FCMs generate a new state vector at each discrete time step, and this procedure is repeated until the system stabilizes. Considering the above, in the example, the proposed FCM model reaches a steady state after 9 iterations and the corresponding state vector is generated, using the weight matrix presented below:

$$w_{ij=}\begin{bmatrix} 0 & 1 & 0.42 & 0.74 & 1 & -0.89 & 0.93 \\ 1 & 0 & 0.48 & 0.95 & 1 & -0.71 & 1 \\ 0.42 & 0.48 & 0 & 0.30 & 0.59 & -1 & 0.22 \\ 0.74 & 0.95 & 0.30 & 0 & 1 & -0.57 & 0.52 \\ 1 & 1 & 0.59 & 1 & 0 & -0.45 & -1 \\ -0.89 & -0.71 & -1 & -0.57 & -0.45 & 0 & -0.21 \\ 0 & 0 & 0 & 0 & 0 & 0 & 0 \end{bmatrix} \tag{13}$$

The resulting state vector is the $A^9$ = (0.95, 0.93, 0.95, 0.95, 0.13, 0.19, 0.97). The last value of $A^9$ corresponds to the output concept $C_7$="*pneumonia*", which is responsible for the outcome of the problem. Figure 4 (a) illustrates the constructed fuzzy sets utilized to linguistically characterize the calculated degree of pneumonia as: "*Very Low* (*VL*)" [0, 0.30], "*Low* (*L*)" [0.20, 0.50], "*Medium* (*M*)" [0.30, 0.70], "*High* (*H*)" [0.50, 0.80], "*Very High* (*VH*)" [0.70, 1]. In this example $A^9$ reveals that the examined patient has a "*Very High*" possibility of having pneumonia, which is equal to 0.97. Specifically, according to the calculated $A^9$, the possibility of pneumonia is "*Very High*" if the following apply:

- the texture of the lung regions in the chest X-ray, described by $C_1$=Right Upper, $C_2$= Left Upper, $C_3$= Right Middle, $C_4$= Left Middle, is "*Very High*". This is because the respective calculated concept values of the graph after 9 iterations are $C_1 = 0.95$, $C_2 = 0.93$, $C_3 = 0.95$, $C_4 = 0.95$ and correspond to "*Very High*" pneumonia, based on the defined fuzzy sets (Figure 4 (a)).
- the texture of the lung regions in the chest x-ray, given by $C_5$= Right Lower, $C_6$= Left Lower is "*Very Low*". This is because the resulting concept values $C_5 = 0.13$, $C_6 = 0.19$ represent "*Very Low*" pneumonia, based on the constructed fuzzy sets illustrated in Figure 4 (a).

In this paper, the texture is characterized by wavelet energy features, as described in section 3.1. This can also be noticed in Figure 3, which depicts a normal lung (Figure 3left) and a lung suffering from pneumonia (Figure 3right). In the case of the lung suffering from pneumonia, the brightness level is more intense with a different texture differentiating the DWT energy levels from those characterizing the normal lung parenchyma. The proposed model is performing its reasoning procedure, until it finally reaches a steady state and converges; the convergence plot of the proposed FCM for a patient suffering from "Very High" pneumonia is depicted in Figure 4 (b). In addition, as observed from the experiments performed, the energy $\bar{e}_u$ corresponding to images from normal patients is lower than those with pneumonia disease; this is because there are fewer light deviations in normal x-rays

## 5 CONCLUCIONS

In this paper, a novel FCM model aiming to perform pneumonia detection. Taking into consideration that diagnosing pneumonia from x-ray images is time consuming and less accurate, the introduced model deals with these problems, whereas it limits human intervention. The experiments demonstrated the effectiveness of the introduced FCM model, as it succeeded in identifying which regions of the lungs were most associated with pneumonia, while automatically detecting the interconnections between them. In addition, the proposed model provides easily explainable results, while being aware of uncertainty, and simple to implement. Future research directions include further investigation of the effectiveness of the proposed model.

## ACKNOWLEDGMENTS

This work was supported in part by the grant No. 5922 of the Special Account of Research Grants of the University of Thessaly, Greece.

## REFERENCES

[1] M. M. Pettigrew, W. Tanner, and A. D. Harris, "The lung microbiome and pneumonia," The Journal of Infectious Diseases, vol. 223, no. Supplement_3, pp. S241–S245, 2021.
[2] K. Stokes, R. Castaldo, C. Federici, S. Pagliara, A. Maccaro, F. Cappuccio, G. Fico, M. Salvatore, M. Franzese, and L. Pecchia, "The use of artificial intelligence systems in diagnosis of pneumonia via signs and symptoms: A systematic review," Biomedical Signal Processing and Control, vol. 72, p. 103325, 2022.
[3] B. Kosko, "Fuzzy cognitive maps," International journal of man-machine studies, vol. 24, no. 1, pp. 65–75, 1986.
[4] G. Felix, G. Nápoles, R. Falcon, W. Froelich, K. Vanhoof, and R. Bello, "A review on methods and software for fuzzy cognitive maps," Artificial intelligence review, vol. 52, no. 3, pp. 1707–1737, 2019.

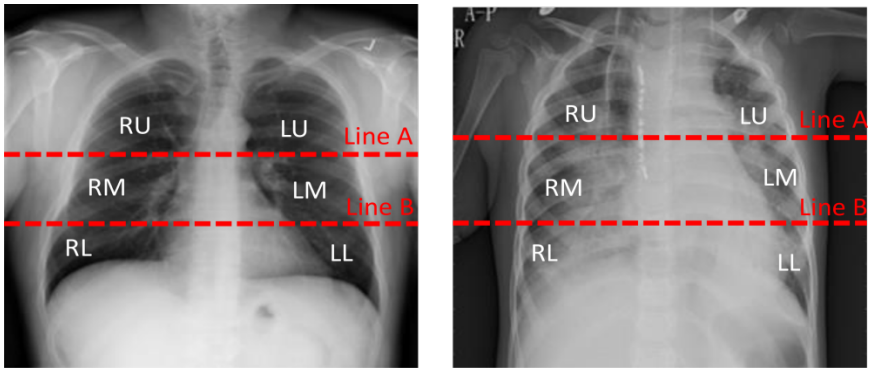


**Figure 3: X-ray of healthy individual (left), and a patient with pneumonia (right).**

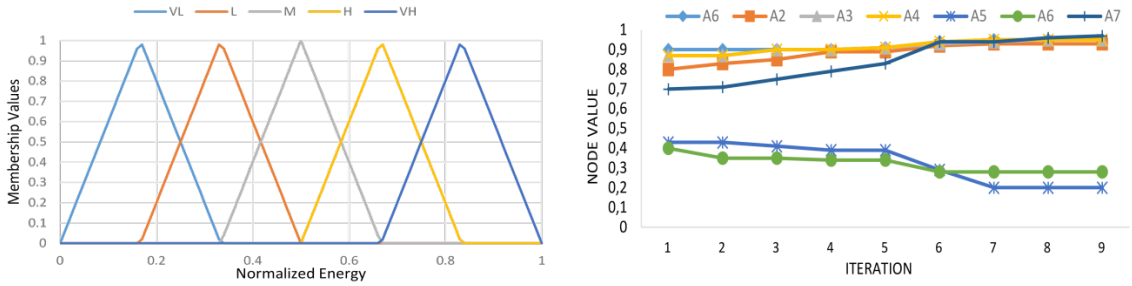


**Figure 4: (Left) Membership functions for pneumonia diagnosis; Very Low (VL), Low (L), Medium (M), High (H), and Very High (VH), (Right) convergence plot of the proposed FCM model for a patient with "Very High" pneumonia.**

[5] C. D. Stylios, V. C. Georgopoulos, G. A. Malandraki, and S. Chouliara, "Fuzzy cognitive map architectures for medical decision support systems," Applied Soft Computing, vol. 8, no. 3, pp. 1243–1251, 2008.
[6] D. K. Iakovidis and E. Papageorgiou, "Intuitionistic Fuzzy Cognitive Maps for Medical Decision Making," IEEE Transactions on Information Technology in Biomedicine, vol. 15, no. 1, pp. 100–107, 2011.
[7] A. Borghesi and R. Maroldi, "COVID-19 outbreak in Italy: experimental chest X-ray scoring system for quantifying and monitoring disease progression," La radiologia medica, vol. 125, no. 5, pp. 509–513, 2020.
[8] G. Sovatzidi, P. Gatoula, M. D. Vasilakakis, and D. K. Iakovidis, "Explainable Fuzzy Texture Words Model for Automatic Bone Fracture Identification," in 2021 IEEE International Conference on Imaging Systems and Techniques (IST), 2021, pp. 1–6.
[9] S. G. Mallat, "A theory for multiresolution signal decomposition: the wavelet representation," IEEE transactions on pattern analysis and machine intelligence, vol. 11, no. 7, pp. 674–693, 1989.
[10] Kovacevic and W. Sweldens, "Wavelet families of increasing order in arbitrary dimensions," IEEE Transactions on Image Processing, vol. 9, no. 3, pp. 480–496, 2000.
[11] M. D. Vasilakakis, D. K. Iakovidis, and G. Koulaouzidis, "A Constructive Fuzzy Representation Model for Heart Data Classification," in Public Health and Informatics, IOS Press, 2021, pp. 13–17.
[12] S. Rachamanee and P. Wongupparaj, "Resting-state EEG datasets of adolescents with mild, minimal, and moderate depression," BMC Research Notes, vol. 14, no. 1, pp. 1–3, 2021.
[13] M. E. Chowdhury, T. Rahman, A. Khandakar, R. Mazhar, M. A. Kadir, Z. B. Mahbub, K. R. Islam, M. S. Khan, A. Iqbal, N. Al Emadi, and others, "Can AI help in screening viral and COVID-19 pneumonia?," IEEE Access, vol. 8, pp. 132665–132676, 2020.
[14] S. Theodoridis and K. Koutroumbas, Pattern Recognition, Fourth Edition, 4th ed. Orlando, FL, USA: Academic Press, Inc., 2008.
[15] T. Fawcett, "An introduction to ROC analysis," Pattern recognition letters, vol. 27, no. 8, pp. 861–874, 2006.